

# Automatic Differentiation is Essential in Training Neural Networks for Solving Differential Equations

Chuqi Chen<sup>a,\*</sup>, Yahong Yang<sup>b,\*</sup>, Yang Xiang<sup>a,c,\*\*</sup>, Wenrui Hao<sup>b,\*\*</sup>

<sup>a</sup>*Department of Mathematics, The Hong Kong University of Science and Technology, Clear Water Bay, Hong Kong Special Administrative Region of China*

<sup>b</sup>*Department of Mathematics, The Pennsylvania State University, USA*

<sup>c</sup>*Algorithms of Machine Learning and Autonomous Driving Research Lab, HKUST Shenzhen-Hong Kong Collaborative Innovation Research Institute, Futian, Shenzhen, China*

---

## Abstract

Neural network-based approaches have recently shown significant promise in solving partial differential equations (PDEs) in science and engineering, especially in scenarios featuring complex domains or the incorporation of empirical data. One advantage of neural network method for PDEs lies in its automatic differentiation (AD), which necessitates only the sample points themselves, unlike traditional finite difference (FD) approximations that require nearby local points to compute derivatives. In this paper, we quantitatively demonstrate the advantage of AD in training neural networks. The concept of truncated entropy is introduced to characterize the training property. Specifically, through comprehensive experimental and theoretical analyses conducted on random feature models and two-layer neural networks, we discover that the defined truncated entropy serves as a reliable metric for quantifying the residual loss of random feature models and the training speed of neural networks for both AD and FD methods. To substantiate our observations, we corroborate our results through the application of random feature methods and the neural network paradigm, respectively.

*Keywords:* Neural network, Differential equation, Automatic differentiation, Numerical differentiation, Training error

---

\*Equal contribution

\*\*Corresponding author

*Email addresses:* maxiang@ust.hk (Yang Xiang), wxh64@psu.edu (Wenrui Hao)

---

## 1. Introduction

Neural networks have been extensively applied in solving partial differential equations (PDEs) [1, 2, 3, 4, 5, 6, 7, 8], particularly in addressing high-dimensional problems, complex domains, and incorporating empirical data. Approaches like Physics-Informed Neural Networks (PINNs) [1, 9, 10] and the deep Ritz method [2, 11] have demonstrated this approach. In solving PDEs, the computation of derivatives within the loss functions is crucial. A long-standing debate exists on how best to handle the differential operator. There are primarily two approaches:

- Automatic Differentiation (AD)[12, 1, 13]: This method leverages the backpropagation capabilities of neural networks to compute derivatives directly. While AD is precise, it can be memory-intensive and time-consuming, particularly for deep neural networks.
- Numerical Differentiation[14, 15, 16, 17, 18, 19, 20, 21]: Techniques like the finite difference method approximate differential operators numerically. Though less accurate and inherently approximate, this approach is easy to implement and computationally less demanding.

To date, there has been limited research directly comparing these methods to determine which is superior, especially from the training perspective, though promising numerical results have been achieved with both. In this paper, we use the finite difference(FD) method as an example of numerical differentiation. We find that there is a significant discrepancy in the training performance between these two differentiation approaches (see Fig. 1 right), with AD outperforming FD. Motivated by this difference, this paper specifically delves into analyzing the training error of these two methods.

In this paper, we compare AD and FD methods for PDEs by training two-layer neural networks and the random feature model (RFM) [7]. Both models follow the same structure as depicted in Eq. 3. The two-layer neural networks (NN) involve training all parameters, whereas the RFM fixes the inner layer parameters randomly and trains only the outer layer parameters. Specifically, the RFM addresses a convex optimization (least squares problem), solving  $\mathbf{A}\mathbf{a} = \mathbf{f}$ , where  $\mathbf{a}$  represents the outer layer parameters, as shown in Eq. 3. We refer to  $\mathbf{A}$  as the system matrix. In contrast, training the two-layer neural

networks involves nonconvex optimization, tackled via gradient descent. The loss dynamics are expressed as  $\frac{\partial L}{\partial t} = -\mathbf{e}^\top \mathbf{G} \mathbf{e}$ , where  $L = \mathbf{e}^2$  denotes the loss function in PDE solving, and  $\mathbf{G}$  represents the kernel of the gradient descent.

Our analysis is grounded in eigenvalue studies in training process, shedding light on the distinct behaviors exhibited by AD and FD in PINN frameworks. We observe that different differentiation methods influence both  $\mathbf{A}$  and  $\mathbf{G}$ , thereby affecting the training process. By analyzing the singular values or eigenvalues of  $\mathbf{A}$  and  $\mathbf{G}$  derived from these differentiation methods, we find that training performance is closely tied to these values. Our theoretical and experimental analyses indicate that AD outperforms FD methods. In RFM, AD achieves a smaller residual error (i.e., training error), as illustrated in Fig. 1(b). In two-layer neural networks, AD facilitates faster gradient descent dynamics compared to FD, leading to a more rapid decrease in the loss function.

Based on theoretical analysis and computational experiments, we observe that the singular values of matrices  $\mathbf{A}$  and  $\mathbf{G}$  exhibit similar characteristics in both the AD and FD methods. Notably, the large singular values are nearly identical due to the relatively small numerical differentiation errors introduced by FD (Proposition. 1). However, we observe that the small singular values of FD are larger than those of AD, primarily due to the impact of numerical differentiation errors on these smaller values (Proposition. 2). Therefore, in the RFM, a truncated singular value approach is necessary to solve  $\mathbf{A}\mathbf{a} = \mathbf{f}$  by computing a pseudoinverse of  $\mathbf{a}$ , where only singular values greater than the truncated value are inverted. Since FD retains more small singular values than AD, this discrepancy leads to higher training errors for FD. These small singular values, while contributing less to approximation error, significantly impact training error, explaining AD's better performance in the RFM. Similarly, in two-layer neural networks, the abundance of small values in  $\mathbf{G}$  for FD slows down the training process in gradient descent methods, resulting in slower training compared to AD.

To quantify this observation, we introduce the following two definitions to measure the number of small singular values near the truncation threshold:

**Definition 1 (Effective cut-off number).** *Let  $\mathbb{S}$  represent the set of singular values of matrix  $\mathbf{A}$  and  $\sigma_{max}$  is the largest singular value of  $\mathbf{A}$ . We define a function  $e_{\mathbf{A}}(a)$  that denotes the count of singular values in set  $\mathbb{S}$  that do not exceed a given value, denoted by  $a \cdot \sigma_{max}$  ( $0 \leq a < 1$ ). Mathematically,*

this can be expressed as:

$$e_{\mathbf{A}}(a) = |\{\sigma \in \mathbb{S} : \sigma \geq a \cdot \sigma_{\max}\}|, \quad (1)$$

where  $|\cdot|$  denotes the cardinality of this set.

Based on the effective cut-off number, we introduce the truncated entropy:

**Definition 2 (Truncated entropy).** For a matrix  $\mathbf{A} \in \mathbb{R}^{m \times n}$  with singular values  $\sigma_1 \geq \sigma_2 \geq \dots \geq \sigma_m$ , and a given  $a \geq 0$ , the truncation entropy of  $\mathbf{A}$  is defined as:

$$H_{\mathbf{A}}(a) = -\frac{1}{\log e_{\mathbf{A}}(a)} \sum_{k=1}^{e_{\mathbf{A}}(a)} p_k \log p_k, \quad (2)$$

where  $p_k = \frac{\sigma_k}{\|\boldsymbol{\sigma}\|_1}$ , for  $k = 1, 2, \dots, e_{\mathbf{A}}(a)$ , with  $\boldsymbol{\sigma} = [\sigma_1, \sigma_2, \dots, \sigma_{e_{\mathbf{A}}(a)}]^T$ .

**Remark 1.** As defined in Definition 2, if all the singular values are equal then  $p_k = \frac{\sigma_k}{\|\boldsymbol{\sigma}\|_1} = \frac{1}{e_{\mathbf{A}}(a)}$  as  $\boldsymbol{\sigma} = [\sigma_1, \dots, \sigma_{e_{\mathbf{A}}(a)}]^T$ . Therefore  $H_{\mathbf{A}}(a) = -\frac{1}{e_{\mathbf{A}}(a)} \sum_{k=1}^{e_{\mathbf{A}}(a)} p_k \log p_k = -\frac{1}{\log e_{\mathbf{A}}(a)} \sum_{k=1}^{e_{\mathbf{A}}(a)} \frac{1}{e_{\mathbf{A}}(a)} \log(\frac{1}{e_{\mathbf{A}}(a)}) = 1$ , which is also the upper bound for the defined truncated entropy due to Gibbs' inequality. The simplicity of computing the pseudo-inverse for matrices with identical eigenvalues is well-captured by the fact that the truncated entropy achieves its maximum under such circumstances.

Note that the defined truncated entropy, which is a normalized version of the spectral entropy [22, 23] after truncation, plays a crucial role in our study. It reflects the impact of small singular values after truncation. Theoretical analysis, presented in Theorem 1 and Remark 3, demonstrates the effectiveness of the defined truncated entropy in quantifying the training speed of gradient descent. Specifically, the larger the value of  $H_{\mathbf{A}}(a)$ , the faster the training speed. Empirically, we observe a strong correlation between truncated entropy and training error, as depicted in Fig. 1. As the number of neurons increases, truncated entropy decreases, leading to an increase in training error. The truncated entropy of AD surpasses that of FD, indicating that AD achieves a lower training error compared to FD.

We delve into a comparative analysis of the performance of automatic differentiation (AD) and finite difference (FD) methods within Physics-Informed Neural Networks (PINN) in Section 3. We present experimental results conducted in higher-dimensional spaces and for higher-order derivative PDEs, to validate our findings and demonstrate the consistency of results across varying dimensions and complexities in Section 4.

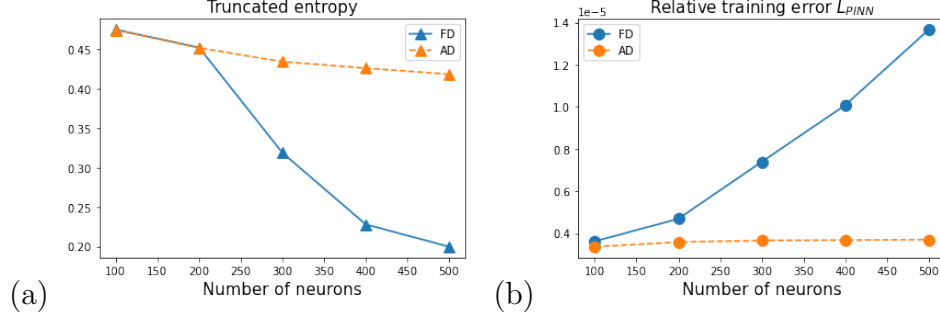


Figure 1: **(a)**: Truncated entropy and **(b)**: Relative training error  $L_{PINN}$  ( $\|\mathbf{A}\mathbf{a} - \mathbf{f}\|/\|\mathbf{f}\|$ ) are depicted for both AD and FD methods with varying numbers of neurons in RFM for solving  $u_{xx} = f(x)$  with Dirichlet boundary conditions. The exact solution is given by  $u(x) = \sin(\pi x)$ , where  $x \in [-1, 1]$ . (The number of sample points equals the number of neurons, and the effective cutoff number is  $e_A(10^{-12})$ ).

## 2. Neural Network Structure and Setups for Solving PDEs

In this section, we review two types of neural network models: two-layer neural networks and random feature models for solving the Poisson equation based on the Physics-Informed Neural Networks (PINNs) method [1]. We will extend our results to other equations in the computational experiments section.

### 2.1. Neural Network Structure

We focus on the two-layer neural network structure operating in a  $d$ -dimensional space, where there is only one hidden layer. The model is represented as:

$$\phi(\mathbf{x}; \boldsymbol{\theta}) = \sum_{j=1}^M a_j \sigma(\mathbf{w}_j \cdot \mathbf{x} + b_j), \quad \mathbf{x} \in \Omega \quad (3)$$

In this neural network,  $\boldsymbol{\theta}$  denotes all the parameters  $\{(a_j, \mathbf{w}_j, b_j)\}_{j=1}^M \subset \mathbb{R} \times \mathbb{R}^d \times \mathbb{R}$ , all of which are free parameters that need to be learned. Here,  $\sigma$  represents the nonlinear activation function. Due to the inherent nonlinearity in this formulation, the learning process becomes nonconvex, posing challenges in optimization.

The random feature model is identical to Eq. 3, except that the inner parameters  $\{\mathbf{w}_j, b_j\}_{j=1}^M$  are randomly chosen and fixed [7]. A common choice

is the uniform distribution  $\mathbf{w}_j \sim \mathbb{U}([-R_m, R_m]^d)$  and  $b_j \sim \mathbb{U}([-R_m, R_m])$ , though different distributions can be used. The outer parameters  $\{a_j\}_{j=1}^M$  are free and the only ones subject to training. Consequently, the training process can be reduced to a convex optimization problem (least squares problem). The approximation capabilities of these two models have been extensively studied in the literature. Notable works include [24, 25, 26, 27], which investigate the approximation ability of neural networks; the approximation capabilities of the random feature model are studied in [28, 29].

## 2.2. PDE-solving Setup

We consider the following Poisson equation:

$$\begin{cases} \Delta u = f & \text{in } \Omega, \\ u = 0 & \text{on } \partial\Omega. \end{cases} \quad (4)$$

Using a neural network structure, the training loss function of PINNs [1] is defined as:

$$L_{\text{PINN}}(\boldsymbol{\theta}) := L_{\text{F}}(\boldsymbol{\theta}) + \lambda L_{\text{B}}(\boldsymbol{\theta}) = \sum_{i=1}^N |\Delta\phi(\mathbf{x}_i; \boldsymbol{\theta}) - f(\mathbf{x})|^2 + \lambda \sum_{i=1}^{\hat{N}} |\phi(\mathbf{y}_i; \boldsymbol{\theta})|^2. \quad (5)$$

Here,  $L_{\text{F}}(\boldsymbol{\theta})$  represents the residual on PDE equations, while  $L_{\text{B}}(\boldsymbol{\theta})$  represents the boundary/initial condition. The variables  $\mathbf{x}_j \in \Omega$  and  $\mathbf{y}_j \in \partial\Omega$ , and  $\lambda$  is a constant used to balance the contributions from the domain and boundary terms.

## 3. AD v.s. FD Methods

When solving PDEs using neural networks, the derivatives appear in the loss function, Eq. 5, and are handled in two approaches: AD computes derivatives analytically via the chain rule [12, 1, 13], while FD approximates derivatives numerically based on local points [14, 15, 16, 17]. In this section, we compare AD and FD methods on the loss function of the PINN setup for both the random feature model and two-layer neural networks. Specifically, we investigate: (1) the truncated entropy of system matrix  $\mathbf{A}$  within the random feature method, and (2) the singular value distribution of the training kernel  $\mathbf{G}$  within the neural network. By analyzing these two models, we can

evaluate how the differentiation methods affect the training process. For simplicity, we employ the one-dimensional Poisson equation  $u_{xx}(x) = f(x)$  with Dirichlet boundary conditions to illustrate our experimental and theoretical analysis. The exact solution of the equation is represented by  $u(x) = \sin(\pi x)$ , where  $x \in [-1, 1]$ .

### 3.1. AD v.s. FD for Random Feature Models

For simplicity, we focus on the differential equation residual loss (since the boundary condition does not involve derivatives) in Eq. 5, namely,

$$L_F(\mathbf{a}) := \sum_{i=1}^N |\phi_{xx}(x_i; \mathbf{a}) - f(x_i)|^2. \quad (6)$$

Here,  $x_i = -1 + i \cdot h$ , where  $h = \frac{2}{N}$ . In this context, since we only need to train the parameters  $\{a_j\}_{j=1}^M$  in the random feature model, we use  $\phi(x; \mathbf{a})$  instead of  $\phi(x; \boldsymbol{\theta})$ .

To compute the second-order derivatives, the loss function with the AD method can be expressed as:

$$L_F^{\text{AD}}(\mathbf{a}) := \sum_{i=1}^N \left| \sum_{j=1}^M a_j w_j^2 (\sigma''(w_j \cdot x_i + b_j) - f(x_i)) \right|^2 = \|\mathbf{A}_{\text{AD}} \cdot \mathbf{a} - \mathbf{f}\|^2, \quad (7)$$

where  $\mathbf{A}_{\text{AD}} = (w_j^2 (\sigma''(w_j \cdot x_i + b_j)))_{ij}$  and  $\mathbf{f} = [f(x_1), f(x_2), \dots, f(x_N)]^T$ . The solution can be computed as  $\mathbf{a} = \mathbf{A}_{\text{AD}}^\dagger \mathbf{f}$ , where  $\mathbf{A}_{\text{AD}}^\dagger = (\mathbf{A}_{\text{AD}}^T \mathbf{A}_{\text{AD}})^{-1} \mathbf{A}_{\text{AD}}^T$  is the pseudo-inverse of  $\mathbf{A}_{\text{AD}}$ .

The loss function with the FD method reads as:

$$\begin{aligned} L_F^{\text{FD}}(\mathbf{a}) &= \sum_{i=1}^N \left| \sum_{j=1}^M a_j \frac{\sigma(w_j \cdot x_{i-1} + b_j) + \sigma(w_j \cdot x_{i+1} + b_j) - 2\sigma(w_j \cdot x_i + b_j)}{h^2} - f(x_i) \right|^2 \\ &= \|\mathbf{A}_{\text{FD}} \cdot \mathbf{a} - \mathbf{f}\|^2, \end{aligned} \quad (8)$$

where  $\mathbf{A}_{\text{FD}} = \mathbf{C}_2 \cdot \mathbf{A}_0$  as shown in Eq. 17 below. The solution can be computed as  $\mathbf{a} = \mathbf{A}_{\text{FD}}^\dagger \mathbf{f}$ , where  $\mathbf{A}_{\text{FD}}^\dagger = (\mathbf{A}_{\text{FD}}^T \mathbf{A}_{\text{FD}})^{-1} \mathbf{A}_{\text{FD}}^T$  is the pseudo-inverse of  $\mathbf{A}_{\text{FD}}$ .

In this section, we will analyze the training process of these two methods based on the singular values of  $\mathbf{A}_{\text{AD}}$  or  $\mathbf{A}_{\text{FD}}$ , i.e., the positive square root of eigenvalues of  $\mathbf{A}_{\text{AD}}^T \mathbf{A}_{\text{AD}}$  and  $\mathbf{A}_{\text{FD}}^T \mathbf{A}_{\text{FD}}$ . First of all, we want to mention that

the large singular values are close for the two matrices since when  $h$  is small, the gap between the two matrices is small, i.e.,

$$\mathbf{A}_{AD} = \mathbf{A}_{FD} + h^2 \mathbf{E}, \quad (9)$$

where  $\mathbf{E}$  is the numerical differentiation errors matrix. Hence, the difference in eigenvalues between the two matrices is  $\mathcal{O}(h^2)$ , which will affect the small singular values a lot but not the large singular values. Mathematically, we can show that

**Proposition 1.** *Suppose  $\mathbf{E}^\top \mathbf{A}_{FD} + \mathbf{A}_{FD}^\top \mathbf{E} + h^2 \mathbf{E}^\top \mathbf{E}$  is positive definite and the largest eigenvalue is  $\bar{\lambda}$ , we have that*

$$\lambda_{\max}(\mathbf{A}_{FD}^\top \mathbf{A}_{FD}) \leq \lambda_{\max}(\mathbf{A}_{AD}^\top \mathbf{A}_{AD}) \leq \lambda_{\max}(\mathbf{A}_{FD}^\top \mathbf{A}_{FD}) + h^2 \bar{\lambda}. \quad (10)$$

*Proof.* First of all, we prove

$$\lambda_{\max}(\mathbf{A}_{AD}^\top \mathbf{A}_{AD}) \leq \lambda_{\max}(\mathbf{A}_{FD}^\top \mathbf{A}_{FD}) + h^2 \bar{\lambda}.$$

Since

$$\mathbf{A}_{AD}^\top \mathbf{A}_{AD} = \mathbf{A}_{FD}^\top \mathbf{A}_{FD} + h^2 (\mathbf{E}^\top \mathbf{A}_{FD} + \mathbf{A}_{FD}^\top \mathbf{E}) + h^4 \mathbf{E}^\top \mathbf{E}, \quad (11)$$

we have

$$[\lambda_{\max}(\mathbf{A}_{FD}^\top \mathbf{A}_{FD}) + h^2 \bar{\lambda}] \cdot \mathbf{I} - \mathbf{A}_{AD}^\top \mathbf{A}_{AD} \quad (12)$$

is a positive definite matrix. For any eigenvalue of  $\mathbf{A}_{AD}^\top \mathbf{A}_{AD}$ ,  $\lambda$ ,  $\mathbf{A}_{AD}^\top \mathbf{A}_{AD} \mathbf{v} = \lambda \mathbf{v}$ , we have

$$[\lambda_{\max}(\mathbf{A}_{FD}^\top \mathbf{A}_{FD}) + h^2 \bar{\lambda}] \cdot \mathbf{I} \cdot \mathbf{v} - \mathbf{A}_{AD}^\top \mathbf{A}_{AD} \mathbf{v} = (\lambda_{\max}(\mathbf{A}_{FD}^\top \mathbf{A}_{FD}) + h^2 \bar{\lambda} - \lambda) \mathbf{v}. \quad (13)$$

Hence

$$\lambda_{\max}(\mathbf{A}_{FD}^\top \mathbf{A}_{FD}) + h^2 \bar{\lambda} - \lambda \geq 0,$$

due to the arbitrary choice of  $\lambda$ , we obtain

$$\lambda_{\max}(\mathbf{A}_{AD}^\top \mathbf{A}_{AD}) \leq \lambda_{\max}(\mathbf{A}_{FD}^\top \mathbf{A}_{FD}) + h^2 \bar{\lambda}.$$

Now we prove the next part, we have

$$\lambda_{\max}(\mathbf{A}_{AD}^\top \mathbf{A}_{AD}) \cdot \mathbf{I} - \mathbf{A}_{FD}^\top \mathbf{A}_{FD} \quad (14)$$

is a positive definite matrix. For any eigenvalue of  $\mathbf{A}_{FD}^\top \mathbf{A}_{FD}$ ,  $\lambda$ ,  $\mathbf{A}_{FD}^\top \mathbf{A}_{FD} \mathbf{v} = \lambda \mathbf{v}$ , we have

$$[\lambda_{\max}(\mathbf{A}_{AD}^\top \mathbf{A}_{AD}) \cdot \mathbf{I} - \mathbf{A}_{FD}^\top \mathbf{A}_{FD}] \mathbf{v} = (\lambda_{\max}(\mathbf{A}_{AD}^\top \mathbf{A}_{AD}) - \lambda) \mathbf{v}. \quad (15)$$



Hence

$$\lambda_{\max}(\mathbf{A}_{\text{FD}}^{\top} \mathbf{A}_{\text{FD}}) - \lambda \geq 0,$$

due to the arbitrary choice of  $\lambda$ , we obtain

$$\lambda_{\max}(\mathbf{A}_{\text{FD}}^{\top} \mathbf{A}_{\text{FD}}) \leq \lambda_{\max}(\mathbf{A}_{\text{AD}}^{\top} \mathbf{A}_{\text{AD}}).$$

□

For the small eigenvalues, based on the following Proposition 2, we know that the small eigenvalue, i.e., the eigenvalue in  $\mathcal{O}(h^2)$  level,  $\mathbf{A}_{\text{AD}}^{\top} \mathbf{A}_{\text{AD}}$ , should be smaller than  $\mathbf{A}_{\text{FD}}^{\top} \mathbf{A}_{\text{FD}}$ .

Denoting  $\mathbf{A}_0 = (\sigma(w_j \cdot x_i + b_j))_{ij}$  and  $\mathbf{A}_2 = (\sigma''(w_j \cdot x_i + b_j))_{ij}$ , we have that

$$\mathbf{A}_{\text{AD}} = \mathbf{A}_2 \cdot \mathbf{D}_2, \quad \mathbf{A}_{\text{FD}} = \mathbf{C}_2 \cdot \mathbf{A}_0 \quad (16)$$

where

$$\mathbf{C}_2 = \frac{1}{h^2} \begin{bmatrix} -2 & 1 & & & \\ 1 & -2 & 1 & & \\ & \ddots & \ddots & \ddots & \\ & & 1 & -2 & 1 \\ & & & 1 & -2 \end{bmatrix} \in \mathbb{R}^{N \times N}, \quad \mathbf{D}_2 = \begin{bmatrix} w_1^2 & & \\ & \ddots & \\ & & w_M^2 \end{bmatrix} \in \mathbb{R}^{M \times M}. \quad (17)$$

**Proposition 2.** Suppose  $M = N$ ,  $\mathbf{A}_{\text{FD}}, \mathbf{A}_{\text{AD}}$  is invertible and

$$C := \frac{\lambda_{\min}(\mathbf{A}_0)}{\lambda_{\min}(\mathbf{A}_2)} \geq \frac{1}{\lambda_{\min}(\mathbf{C}_2) \lambda_{\min}(\mathbf{D}_2^{-1})}, \quad (18)$$

then we have

$$\lambda_{\min}(\mathbf{A}_{\text{FD}}) \geq \lambda_{\min}(\mathbf{A}_{\text{AD}}). \quad (19)$$

*Proof.* First of all, we show that

$$\lambda_{\min}(\mathbf{A}_{\text{FD}}) \geq \lambda_{\min}(\mathbf{A}_0) \lambda_{\min}(\mathbf{C}_2), \quad \lambda_{\min}(\mathbf{A}_2) \geq \lambda_{\min}(\mathbf{A}_{\text{AD}}) \lambda_{\min}(\mathbf{D}_2^{-1}). \quad (20)$$

We know that for the symmetric positive definite matrices  $\mathbf{A}$  and  $\mathbf{B}$ ,  $\lambda_{\max}$  is a kind of sub-multiplicative norm, i.e.,

$$\lambda_{\max}(\mathbf{AB}) \leq \lambda_{\max}(\mathbf{A}) \lambda_{\max}(\mathbf{B}).$$

By taking the inverse, we have

$$\lambda_{\min}(\mathbf{A}\mathbf{B}) \geq \lambda_{\min}(\mathbf{A})\lambda_{\min}(\mathbf{B}).$$

Therefore, we have

$$\begin{aligned}\lambda_{\min}(\mathbf{A}_{\text{FD}}^{\top}\mathbf{A}_{\text{FD}}) &= \lambda_{\min}(\mathbf{A}_0^{\top}\mathbf{C}^{\top}\mathbf{C}_2\mathbf{A}_0) = \lambda_{\min}(\mathbf{C}_2\mathbf{A}_0\mathbf{A}_0^{\top}\mathbf{C}^{\top}) \\ &\leq \lambda_{\min}(\mathbf{A}_0\mathbf{A}_0^{\top})\lambda_{\min}^2(\mathbf{C}_2).\end{aligned}$$

thus

$$\lambda_{\min}(\mathbf{A}_{\text{FD}}) \geq \lambda_{\min}(\mathbf{A}_0)\lambda_{\min}(\mathbf{C}_2).$$

The other inequality is proved in the same way.

Based on definition of  $C$ , we have

$$\lambda_{\min}(\mathbf{A}_{\text{FD}}) \geq C\lambda_{\min}(\mathbf{C}_2)\lambda_{\min}(\mathbf{D}_2^{-1})\lambda_{\min}(\mathbf{A}_{\text{AD}}).$$

Due to  $C \geq \frac{1}{\lambda_{\min}(\mathbf{C}_2)\lambda_{\min}(\mathbf{D}_2^{-1})}$ , we have  $\lambda_{\min}(\mathbf{A}_{\text{FD}}) \geq \lambda_{\min}(\mathbf{A}_{\text{AD}})$ .  $\square$

**Remark 2.** In the above proposition, we assume (18), which is reasonable if we omit the effect of the activation function. For smooth functions like  $\sin(x)$  and  $\arctan(x)$ , the eigenvalues of the derivative matrix are of the same order of magnitude as those of the original matrix. In other words, we have  $\lambda_{\min}(\mathbf{A}_0) = C\lambda_{\min}(\mathbf{A}_2)$ , where  $C$  is close to 1. Since  $\lambda_{\min}(\mathbf{C}_2) = 4N^2 \cos^2 \frac{N\pi}{2N+1} > 1$  [30], and  $\lambda_{\min}(\mathbf{D}_2^{-1}) > 1$  if we randomly choose  $w_i \sim \mathbb{U}((-1, 1)^d)$ , Eq. (18) will hold.

We conducted experiments using the random feature method, where we varied the activation functions and dimensions to solve the Poisson equation. Here we choose  $w_j$  and  $b_j$  from uniform distribution  $\mathbb{U}([-1, 1])$ . As depicted in Fig. 2, we observe that the large singular values of  $\mathbf{A}_{\text{FD}}$  and  $\mathbf{A}_{\text{AD}}$  are close, but the small eigenvalue of  $\mathbf{A}_{\text{FD}}$  is larger than  $\mathbf{A}_{\text{AD}}$  confirming the analysis presented earlier.

The distinction between the AD and FD methods in solving PDEs using random feature models can be elucidated by analyzing the differential characteristics of the singular values of  $\mathbf{A}_{\text{AD}}$  and  $\mathbf{A}_{\text{FD}}$ . Minimizing  $L_F^{\text{AD}}(\mathbf{a})$  and  $L_F^{\text{FD}}(\mathbf{a})$  can be reformulated as solving the linear systems  $\mathbf{A}_{\text{AD}}\mathbf{a} = \mathbf{f}$  and  $\mathbf{A}_{\text{FD}}\mathbf{a} = \mathbf{f}$ , respectively. To solve  $\mathbf{A}\mathbf{a} = \mathbf{f}$ , it is often necessary to compute the pseudo-inverse of matrix  $\mathbf{A}$ . However, if the non-zero singular values are too small, the computation error becomes large. To mitigate computation

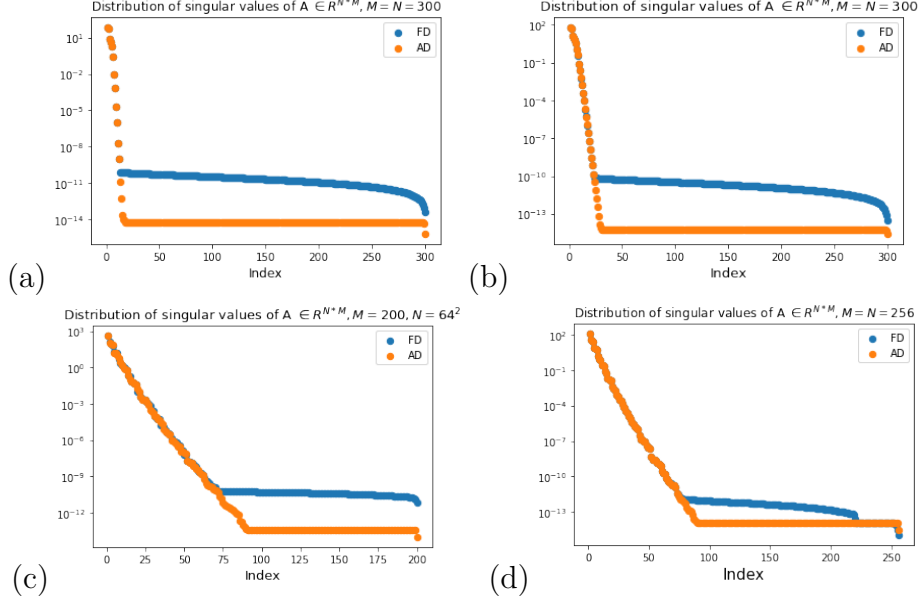


Figure 2: Distribution of singular values for  $\mathbf{A}_{\text{FD}}$  and  $\mathbf{A}_{\text{AD}}$  for solving Poisson equation using Random Feature Method with vary Dimensions  $d$ , Activation Functions  $\sigma(x)$ , Number of Sample Points  $N$  and Number of Neurons  $M$ . **(a):**  $d = 1$ ,  $\sigma(x) = \sin(x)$ ,  $M = N = 100$ . **(b):**  $d = 1$ ,  $\sigma(x) = \tanh(x)$ ,  $M = N = 300$ . **(c):**  $d = 2$ ,  $\sigma(x) = \sin(x)$ ,  $M = 200$ ,  $N = 64 \times 64$ . **(d):**  $d = 2$ ,  $\sigma(x) = \sin(x)$ ,  $M = N = 16 \times 16$ .

errors, it is common practice to do truncation based on singular values of matrix  $\mathbf{A}$ . In this study, we utilize the truncated SVD method to analyze the influence of eigenvalues on the training error. We denote the singular values of  $\mathbf{A}_{\text{AD}}$  as  $\{\sigma_i\}_{i=1}^M$  and those of  $\mathbf{A}_{\text{FD}}$  as  $\{\hat{\sigma}_i\}_{i=1}^M$ . The SVD decomposition of  $\mathbf{A}_{\text{AD}}$  and  $\mathbf{A}_{\text{FD}}$  can be expressed as follows:

$$\mathbf{A}_{\text{AD}} = \sum_{i=1}^P \sigma_i u_i v_i^T + \sum_{i=K+1}^M \sigma_i u_i v_i^T, \quad \mathbf{A}_{\text{FD}} = \sum_{i=1}^{\hat{P}} \hat{\sigma}_i \hat{u}_i \hat{v}_i^T + \sum_{i=\hat{K}+1}^M \hat{\sigma}_i \hat{u}_i \hat{v}_i^T, \quad (21)$$

where  $P$  and  $\hat{P}$  are the truncated positions. Then the truncated matrix can be expressed as  $\tilde{\mathbf{A}}_{\text{AD}} = \sum_{i=1}^P \sigma_i u_i v_i^T$ ,  $\tilde{\mathbf{A}}_{\text{FD}} = \sum_{i=1}^{\hat{P}} \hat{\sigma}_i \hat{u}_i \hat{v}_i^T$ . By direct

calculation, the truncation error can be expressed as

$$\epsilon_{\text{AD}} := \left\| \mathbf{A}_{\text{AD}} - \tilde{\mathbf{A}}_{\text{AD}} \right\|^2 = \sum_{i=P+1}^M \sigma_i^2, \quad \epsilon_{\text{FD}} = \left\| \mathbf{A}_{\text{FD}} - \tilde{\mathbf{A}}_{\text{FD}} \right\|^2 = \sum_{i=\hat{P}+1}^M \hat{\sigma}_i^2.$$

Thus the training error can be formulated as

$$\begin{aligned} \left\| \mathbf{A}_{\text{AD}} \cdot \mathbf{a} - \mathbf{f} \right\|^2 &\leq \left\| \tilde{\mathbf{A}}_{\text{AD}} \cdot \mathbf{a} - \mathbf{f} \right\|^2 + \epsilon_{\text{AD}} \left\| \mathbf{a} \right\|^2, \\ \left\| \mathbf{A}_{\text{FD}} \cdot \mathbf{a} - \mathbf{f} \right\|^2 &\leq \left\| \tilde{\mathbf{A}}_{\text{FD}} \cdot \mathbf{a} - \mathbf{f} \right\|^2 + \epsilon_{\text{FD}} \left\| \mathbf{a} \right\|^2. \end{aligned} \quad (22)$$

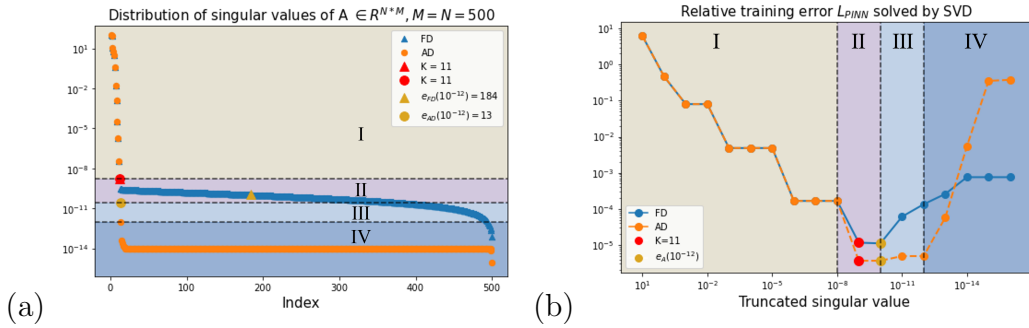


Figure 3: **(a)**: The distribution of singular values alongside their respective truncation positions. Yellow dots represent truncated positions based on  $e_{\mathbf{A}}(10^{-12})$ , with *truncated entropy* values of  $H_{\mathbf{A}_{\text{FD}}}(10^{-12}) = 0.1995$  and  $H_{\mathbf{A}_{\text{AD}}}(10^{-12}) = 0.4183$ . **(b)**: Relative training error of  $L_{\text{PINN}}$ , denoted as  $\frac{\|\mathbf{A}\mathbf{a} - \mathbf{f}\|}{\|\mathbf{f}\|}$ , obtained using the truncated singular value decomposition (SVD) method. The horizontal axis represents the truncation position determined by the effective cut-off number.

The experiment results are shown in Fig. 3. We determine the truncated positions based on *effective cut-off number*, i.e.,  $P = e_{\mathbf{A}_{\text{AD}}}(a)$  and  $\hat{P} = e_{\mathbf{A}_{\text{FD}}}(a)$ . We can divide the truncated position into four stages based on the relationship between training error and the truncated position. In **Stage I**, the truncated position  $P = \hat{P} < K$ , where  $K$  represents the last similar singular value shared by  $\mathbf{A}_{\text{AD}}$  and  $\mathbf{A}_{\text{FD}}$ , as indicated by the red dot in Fig. 3(a). The training errors for AD and FD are similar in this stage because the training error is dominated by  $\epsilon_{\text{AD}} \approx \sum_{i=P+1}^K \sigma_i^2 \approx \epsilon_{\text{FD}} \approx \sum_{i=P+1}^K \hat{\sigma}_i^2$ . In **Stage II**, the truncated position  $P \geq K$ . The red and yellow data points in the Fig. 3(b), the training error of AD is smaller than FD. The

training error is dominated by  $\epsilon_{\text{AD}} \approx \sum_{i=P+1}^M \sigma_i^2 < \epsilon_{\text{FD}} \approx \sum_{i=P+1}^M \hat{\sigma}_i^2$ . In **Stage III** and **Stage IV**, we observe that increasing the truncation position  $P$  leads to an increase in training error. At this time, the training error is dominated by  $\|\tilde{\mathbf{A}}_{\text{AD}} \cdot \mathbf{a} - \mathbf{f}\|^2$  and  $\|\tilde{\mathbf{A}}_{\text{FD}} \cdot \mathbf{a} - \mathbf{f}\|^2$  caused by computation errors that arise when computing the pseudo-inverse of the truncated matrix. The yellow dot in the Fig. 3 represents  $P = e_{\mathbf{A}}(10^{-12})$ , which indicates the truncated position that can be computed without introducing significant computational errors when using the SVD method. If  $P > e_{\mathbf{A}}(10^{-12})$ , it would lead to substantial computational errors. Therefore, we can say that in the given scenario, the effective cut-off number is  $e_{\mathbf{A}}(10^{-12})$ . By calculating the corresponding truncated entropy we have  $H_{\mathbf{A}_{\text{AD}}}(10^{-12}) = 0.4183 > H_{\mathbf{A}_{\text{FD}}}(10^{-12}) = 0.1995$ . The truncated entropy of AD is larger than that of FD. i.e,  $H_{\mathbf{A}_{\text{AD}}}(10^{-12}) > H_{\mathbf{A}_{\text{FD}}}(10^{-12})$ , and AD exhibits a smaller training error compared to FD.

The variation of training error with the truncated position in the Truncated SVD method can provide insights for training in the following neural network case.

### 3.2. AD v.s. FD for two-layer Neural Networks

In contrast to random feature models, for neural networks, the parameters in the activation functions are free, and we cannot directly solve the optimization problem using methods like  $\mathbf{A}\mathbf{a} = \mathbf{f}$ , as this problem is non-convex. To tackle such optimization problems, there are various methods available, including gradient descent [31], stochastic gradient descent [32], Adam method [33], Gauss-Newton method [34], preconditioned methods [35], homotopy methods [36], and others. Each of these methods has its pros and cons, and the choice of method depends on the specific characteristics of the optimization problem and the desired properties of the solution. Here our analysis is based on the gradient descent method.

Due to the structure of neural networks, there are two kinds of parameters: one is outside the activation functions, i.e.,  $\{a_j\}_{j=1}^M$ , and the other is inside the activation function,  $\{w_j, b_j\}_{j=1}^M$  (Eq. 3). For parameters  $\{a_j\}_{j=1}^M$ , the gradient descent can be expressed as:

$$\frac{d\mathbf{a}}{dt} = -2\mathbf{A}_{\kappa}^{\text{T}}(\Delta_{\kappa}\phi(\mathbf{x}; \boldsymbol{\theta}) - f(\mathbf{x})), \quad (23)$$

where  $\mathbf{A}_{\kappa} = \mathbf{A}_{\text{AD}}$  for AD method and  $\mathbf{A}_{\kappa} = \mathbf{A}_{\text{FD}}$  for FD method. For the parameter  $\{w_i, b_i\}_{i=1}^M$ , we only consider  $w_i$  since  $b_i$  can be merged into  $w_i$  by

setting  $\mathbf{x} = (x, 1)$ . The gradient descent of AD methods can be expressed as:

$$\frac{d\mathbf{w}}{dt} = -2(\mathbf{X} \cdot \mathbf{A}_3 \cdot \mathbf{D}_3 \cdot \bar{\mathbf{A}} + 2\mathbf{A}_2 \cdot \mathbf{D}_1 \cdot \bar{\mathbf{A}})^\top \cdot (\Delta_\kappa \phi(\mathbf{x}; \boldsymbol{\theta}) - f(\mathbf{x})), \quad (24)$$

where  $\mathbf{A}_3 = (\sigma^{(3)}(w_j \cdot x_i + b_j))_{ij}$ ,  $\bar{\mathbf{A}} = \text{diag}(a_1, \dots, a_M)$  and  $\mathbf{X} = \text{diag}(x_1, \dots, x_N)$ . For gradient descent in FD method, it can be expressed as:

$$\frac{d\mathbf{w}}{dt} = -2(\mathbf{C}_2 \cdot \mathbf{X} \cdot \mathbf{A}_1 \cdot \bar{\mathbf{A}})^\top (\Delta_\kappa \phi(\mathbf{x}; \boldsymbol{\theta}) - f(\mathbf{x})). \quad (25)$$

For the loss function  $L_F(\boldsymbol{\theta}) := \sum_{i=1}^N |\Delta_\kappa \phi(x_i; \boldsymbol{\theta}) - f(x_i)|^2$ . The gradient descent dynamics can be expressed as:

$$\frac{dL_F(\boldsymbol{\theta})}{dt} = \nabla_{\mathbf{a}} L_F(\boldsymbol{\theta}) \frac{d\mathbf{a}}{dt} + \nabla_{\mathbf{w}} L_F(\boldsymbol{\theta}) \frac{d\mathbf{w}}{dt} = -2(\Delta_\kappa \phi(\mathbf{x}; \boldsymbol{\theta}) - f(\mathbf{x}))^\top \mathbf{G}_\kappa (\Delta_\kappa \phi(\mathbf{x}; \boldsymbol{\theta}) - f(\mathbf{x})),$$

where

$$\begin{aligned} \mathbf{G}_{\text{AD}} &= \mathbf{A}_{\text{AD}} \mathbf{A}_{\text{AD}}^\top + (\mathbf{X} \cdot \mathbf{A}_3 \cdot \mathbf{D}_3 \cdot \bar{\mathbf{A}} + 2\mathbf{A}_2 \cdot \mathbf{D}_1 \cdot \bar{\mathbf{A}})(\mathbf{X} \cdot \mathbf{A}_3 \cdot \mathbf{D}_3 \cdot \bar{\mathbf{A}} + 2\mathbf{A}_2 \cdot \mathbf{D}_1 \cdot \bar{\mathbf{A}})^\top, \\ \mathbf{G}_{\text{FD}} &= \mathbf{A}_{\text{FD}} \mathbf{A}_{\text{FD}}^\top + (\mathbf{C}_2 \cdot \mathbf{X} \cdot \mathbf{A}_1 \cdot \bar{\mathbf{A}})(\mathbf{C}_2 \cdot \mathbf{X} \cdot \mathbf{A}_1 \cdot \bar{\mathbf{A}})^\top. \end{aligned} \quad (26)$$

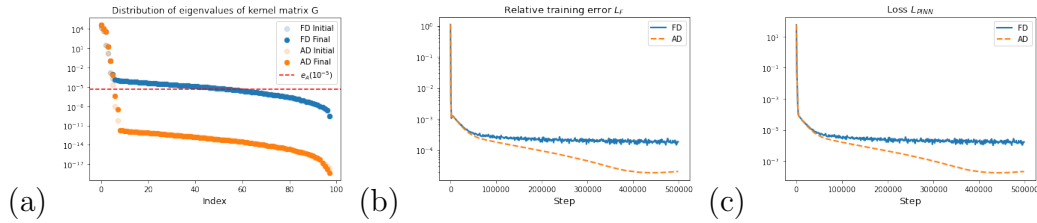


Figure 4: **(a)**: Distribution of eigenvalues of kernel matrix  $G$  with the red dashed line indicating the approximate convergence position  $e_{G_k}(10^{-5})$  at the end of training. *Truncated entropy* values are  $H_{\mathbf{G}_{\text{FD}}}(10^{-5}) = 0.5785$  and  $H_{\mathbf{G}_{\text{AD}}}(10^{-5}) = 0.2606$ . **(b)**: Training curve of relative training error  $\frac{L_F}{\|\mathbf{f}\|}$ . **(c)**: Training curve of the loss function  $L_{\text{PINN}}$ . (Similar performance observed for  $L_F$  and  $L_{\text{PINN}}$  due to the boundary conditions being treated as an identity operator.)

As depicted in Fig. 4(a), the eigenvalues of the kernel  $\mathbf{G}$  in the gradient descent process for learning  $\boldsymbol{\theta}$  exhibit similarities to those of system matrix  $\mathbf{A}$  observed in the random feature model case. This is expected, given that

the kernels  $\mathbf{G}_\kappa$  tend to converge as  $h$  diminishes, reducing the magnitude of large eigenvalues (Proposition 1). Additionally,  $\mathbf{C}_2$  in Eq. 17 serves to augment the small eigenvalues of the kernel in the finite difference (FD) method, surpassing those in the automatic differentiation (AD) methods (Proposition 2). A similar analysis applies to  $\mathbf{A}_\kappa$ , and we refrain from elaborating further here. While the kernel undergoes changes during training, unlike in the random feature model, it's noteworthy that the eigenvalue relationship between the two methods remains consistent throughout training, as illustrated in Fig. 4(a). Based on Fig. 4(b), we can notice that in the beginning of the gradient descent, the performances of AD and FD methods are similar, which is due to the dominant role played by the large eigenvalues, that are similar. After several iteration steps in gradient descent, we notice that the speed of gradient descent in FD is slower than that of AD. This is due to the small eigenvalue direction beginning to play an important role in the training, and we can explain this theoretically as follows.

For the vector  $\mathbf{r}_{\text{AD}} := \Delta_{\text{AD}}\phi(\mathbf{x}; \boldsymbol{\theta}) - f(\mathbf{x})$ , we perform the eigenvalue decomposition of  $\mathbf{A}_{\text{AD}}^\top \mathbf{A}_{\text{AD}}$ , denoted as  $\mathbf{r}_{\text{AD}} = \sum_{i=1}^M \mathbf{r}_{i,\text{AD}}$  such that  $\mathbf{A}_{\text{AD}} \mathbf{A}_{\text{AD}}^\top \mathbf{r}_{i,\text{AD}} = \lambda_{i,\text{AD}} \mathbf{r}_{i,\text{AD}}$  for  $\lambda_{1,\text{AD}} \geq \lambda_{2,\text{AD}} \geq \dots \geq \lambda_{M,\text{AD}}$ . Similarly, for finite difference method, we have  $\mathbf{r}_{\text{FD}} := \Delta_{\text{FD}}\phi(\mathbf{x}; \boldsymbol{\theta}) - f(\mathbf{x}) = \sum_{i=1}^M \mathbf{r}_{i,\text{FD}}$  such that  $\mathbf{A}_{\text{FD}} \mathbf{A}_{\text{FD}}^\top \mathbf{r}_{i,\text{FD}} = \lambda_{i,\text{FD}} \mathbf{r}_{i,\text{FD}}$  for  $\lambda_{1,\text{FD}} \geq \lambda_{2,\text{FD}} \geq \dots \geq \lambda_{M,\text{FD}}$ . Therefore, the gradient descent for two methods can be written as  $\frac{dL_\kappa(\boldsymbol{\theta})}{dt} = -2 \sum_{i=1}^M \lambda_{i,\kappa} \mathbf{r}_{i,\kappa}^2$ . For eigenvalues smaller than  $a\sqrt{\lambda_1}$ , the training error can be considered negligible. This is similar to the truncated SVD in RFM, as shown in Fig. 3, the singular values  $\sigma < 10^{-12}\sigma_1$  can be truncated, given that the training error will not decrease post-truncation. Specifically,  $\mathbf{r}_{i,\text{FD}} \approx 0$  for  $i > e_{\mathbf{G}_{\text{FD}}}(a)$  and  $\mathbf{r}_{i,\text{AD}} \approx 0$  for  $i > e_{\mathbf{G}_{\text{AD}}}(a)$  throughout the entire learning process. Due to the similar performance of  $\mathbf{A}_\kappa$  and  $\mathbf{G}_\kappa$ , we assume the error in this part to be 0 in the gradient descent. This means we disregard these eigenvalues when determining loss convergence speed. Since large eigenvalues (for  $i > e_{\mathbf{G}_\kappa}(b)$ ) converge fast, we consider the stage when the convergence speed is dominated by gradient descent of the kept small eigenvalues, i.e.,  $\frac{dL_\kappa(\boldsymbol{\theta})}{dt} = -2 \sum_{i=e_{\mathbf{G}_\kappa}(b)}^{e_{\mathbf{G}_\kappa}(a)} \lambda_{i,\kappa} \mathbf{r}_{i,\kappa}^2$ . As stated in the following theorem:

**Theorem 1.** *Suppose there exist a constant  $a, b, t_*$  such that  $\mathbf{r}_{i,\text{FD}} = 0$  for  $i > e_{\mathbf{G}_{\text{FD}}}(a)$ ,  $i < e_{\mathbf{G}_{\text{FD}}}(b)$ , and  $\mathbf{r}_{i,\text{AD}} = 0$  for  $i > e_{\mathbf{G}_{\text{AD}}}(a)$ ,  $i < e_{\mathbf{G}_{\text{AD}}}(b)$  for all*

$t \geq t_*$ . For any  $T \geq t_*$ , we have that

$$\begin{aligned} & \exp \left( -2\zeta_\kappa(T) \cdot \max_{t \in [t_*, T]} \frac{\sum_{i=e_{\mathbf{G}_\kappa}(b)}^{e_{\mathbf{G}_\kappa}(a)} \lambda_{i,\kappa}}{e_{\mathbf{G}_\kappa}(a) - e_{\mathbf{G}_\kappa}(b)} (t - t_*) \right) \cdot L_\kappa(\boldsymbol{\theta})[t_*] \\ & \leq L_\kappa(\boldsymbol{\theta})[t] \leq \exp \left( -2\eta_\kappa(T) \cdot \min_{t \in [t_*, T]} \frac{\sum_{i=e_{\mathbf{G}_\kappa}(b)}^{e_{\mathbf{G}_\kappa}(a)} \lambda_{i,\kappa}}{e_{\mathbf{G}_\kappa}(a) - e_{\mathbf{G}_\kappa}(b)} (t - t_*) \right) \cdot L_\kappa(\boldsymbol{\theta})[t_*], \end{aligned} \quad (27)$$

for all  $t \in [t_*, T]$ , where  $\kappa = AD, FD$ , and

$$\eta_\kappa(T) = \min_{t \in [t_*, T]} \frac{\min\{\mathbf{r}_{i,\kappa}^2\}_{i=e_{\mathbf{G}_\kappa}(b)}^{e_{\mathbf{G}_\kappa}(a)}}{\max\{\mathbf{r}_{i,\kappa}^2\}_{i=e_{\mathbf{G}_\kappa}(a)}^{e_{\mathbf{G}_\kappa}(b)}}, \quad \zeta_\kappa(T) := \max_{t \in [t_*, T]} \frac{\max\{\mathbf{r}_{i,\kappa}^2\}_{i=e_{\mathbf{G}_\kappa}(b)}^{e_{\mathbf{G}_\kappa}(a)}}{\min\{\mathbf{r}_{i,\kappa}^2\}_{i=e_{\mathbf{G}_\kappa}(a)}^{e_{\mathbf{G}_\kappa}(b)}}.$$

*Proof.* Due to  $\frac{dL_\kappa(\boldsymbol{\theta})}{dt} = -2 \sum_{i=1}^M \lambda_{i,\kappa} \mathbf{r}_{i,\kappa}^2$  and  $\mathbf{r}_{i,\kappa} = 0$  for  $i > e_{\mathbf{G}_\kappa}(a)$ ,  $i < e_{\mathbf{G}_\kappa}(b)$ , we have that

$$\begin{aligned} \frac{dL_\kappa(\boldsymbol{\theta})}{dt} &= -2 \sum_{i=e_{\mathbf{G}_\kappa}(b)}^{e_{\mathbf{G}_\kappa}(a)} \lambda_{i,\kappa} \mathbf{r}_{i,\kappa}^2 \\ &= \frac{-2 \sum_{i=e_{\mathbf{G}_\kappa}(b)}^{e_{\mathbf{G}_\kappa}(a)} \lambda_{i,\kappa} \mathbf{r}_{i,\kappa}^2}{\sum_{i=e_{\mathbf{G}_\kappa}(b)}^{e_{\mathbf{G}_\kappa}(a)} \mathbf{r}_{i,\kappa}^2} L_\kappa(\boldsymbol{\theta}) \\ &\leq -2 \frac{\min\{\mathbf{r}_{i,\kappa}^2\}_{i=e_{\mathbf{G}_\kappa}(b)}^{e_{\mathbf{G}_\kappa}(a)}}{\max\{\mathbf{r}_{i,\kappa}^2\}_{i=e_{\mathbf{G}_\kappa}(a)}^{e_{\mathbf{G}_\kappa}(b)}} \cdot \frac{\sum_{i=e_{\mathbf{G}_\kappa}(b)}^{e_{\mathbf{G}_\kappa}(a)} \lambda_{i,\kappa}}{e_{\mathbf{G}_\kappa}(a) - e_{\mathbf{G}_\kappa}(b)} L_\kappa(\boldsymbol{\theta}) \\ &\leq -2\eta_\kappa(T) \cdot \min_{t \in [t_*, T]} \frac{\sum_{i=e_{\mathbf{G}_\kappa}(b)}^{e_{\mathbf{G}_\kappa}(a)} \lambda_{i,\kappa}}{e_{\mathbf{G}_\kappa}(a) - e_{\mathbf{G}_\kappa}(b)} \cdot L_\kappa(\boldsymbol{\theta}). \end{aligned} \quad (28)$$

Therefore, we have that

$$L_\kappa(\boldsymbol{\theta})[t] \leq \exp \left( -2\eta_\kappa(T) \cdot \min_{t \in [0, T]} \frac{\sum_{i=e_{\mathbf{G}_\kappa}(b)}^{e_{\mathbf{G}_\kappa}(a)} \lambda_{i,\kappa}}{e_{\mathbf{G}_\kappa}(a) - e_{\mathbf{G}_\kappa}(b)} (t - t_*) \right) \cdot L_\kappa(\boldsymbol{\theta})[t_*] \quad (29)$$

for all  $t \in [t_*, T]$ . The proof for the other direction follows the same steps.  $\square$



**Remark 3.** All the terms in Theorem 1 change with respect to the time  $t$  during the training. Suppose for the two methods,  $\eta_{AD}(T), \zeta_{AD}(T)$  and  $\eta_{FD}(T), \zeta_{FD}(T)$  are close, we can know that the speed of the AD method is faster than the FD methods due to when  $e_G(10^{-5}) > i > e_G(10^{-4})$  as shown in Fig. 4,

$$\frac{\log e_{G_{AD}} H_{G_{AD}}(a)}{e_{G_{AD}}} \approx \frac{\sum_{i=e_{G_{AD}}(b)}^{e_{G_{AD}}(a)} \lambda_{i,AD}}{e_{G_{AD}}(a) - e_{G_{AD}}(b)} \gg \frac{\sum_{i=e_{G_{FD}}(b)}^{e_{G_{FD}}(a)} \lambda_{i,FD}}{e_{G_{FD}}(a) - e_{G_{FD}}(b)} \approx \frac{\log e_{G_{FD}} H_{G_{FD}}(a)}{e_{G_{FD}}}$$

during the training process. This means that Truncated entropy can serve as an indicator of loss convergence speed.

#### 4. Numerical Results

In this section, we apply both the random feature models (RFM) and two-layer Neural Networks(NN) methods discussed in Section.3.1 and Section.3.2 to the Poisson equation in 2D and a fourth-order equation in 1D. This will demonstrate the effectiveness of AD compared to FD. In the case of the random feature model, the system precision is set to double, while for the neural network model, the system precision is set to float. To maintain consistency with our analysis, we train neural networks using the SGD optimizer with full batch training. Detailed experimental setups are provided in the appendix.

**Poisson Equation in 2D.** Consider the Poisson equation in 2D with the Dirichlet boundary condition over  $\Omega = [0, 1] \times [0, 1]$ , namely,

$$\begin{aligned} -\Delta u(x, y) &= f(x, y), \quad (x, y) \in \Omega, \\ u(x, y) &= 0, \quad (x, y) \in \partial\Omega. \end{aligned} \tag{30}$$

By choosing  $f(x) = \pi^2 \sin(\pi x) \sin(\pi y)$ , we have the exact solution is  $u(x, y) = \sin(\pi x) \sin(\pi y)$ . RFM and NN use the same finite difference scheme in the FD case. In the neural network case, the loss function  $L_{PINN}^{AD}(\theta)$  and  $L_{PINN}^{FD}(\theta)$  are defined as follow:

$$L_{PINN}^{AD}(\theta) := L_F^{AD}(\theta) + \lambda L_B(\theta) = \frac{1}{N} \sum_{i=1}^N |\Delta \phi_{xx}(x_i; \theta) - f(x)|^2 + \lambda \frac{1}{\hat{N}} \sum_{i=1}^{\hat{N}} |\phi(y_i; \theta)|^2, \tag{31}$$

$$\begin{aligned}
L_{\text{PINN}}^{\text{FD}}(\boldsymbol{\theta}) &:= L_{\text{F}}^{\text{FD}}(\boldsymbol{\theta}) + \lambda L_{\text{B}}(\boldsymbol{\theta}) \\
&= \frac{1}{N} \sum_{i=1}^N \left| \frac{\phi_{i+1,j} + \phi_{i-1,j} + \phi_{i,j-1} + \phi_{i,j+1} - \phi_{i,j}}{h^2} - f(x_i) \right|^2 + \lambda \frac{1}{\hat{N}} \sum_{i=1}^{\hat{N}} |\phi(\mathbf{y}_i; \boldsymbol{\theta})|^2,
\end{aligned} \tag{32}$$

where  $\lambda = 1$  and  $h = \frac{1}{300}$  and  $\phi_{i,j} := \phi((x_i, y_j); \boldsymbol{\theta})$ .

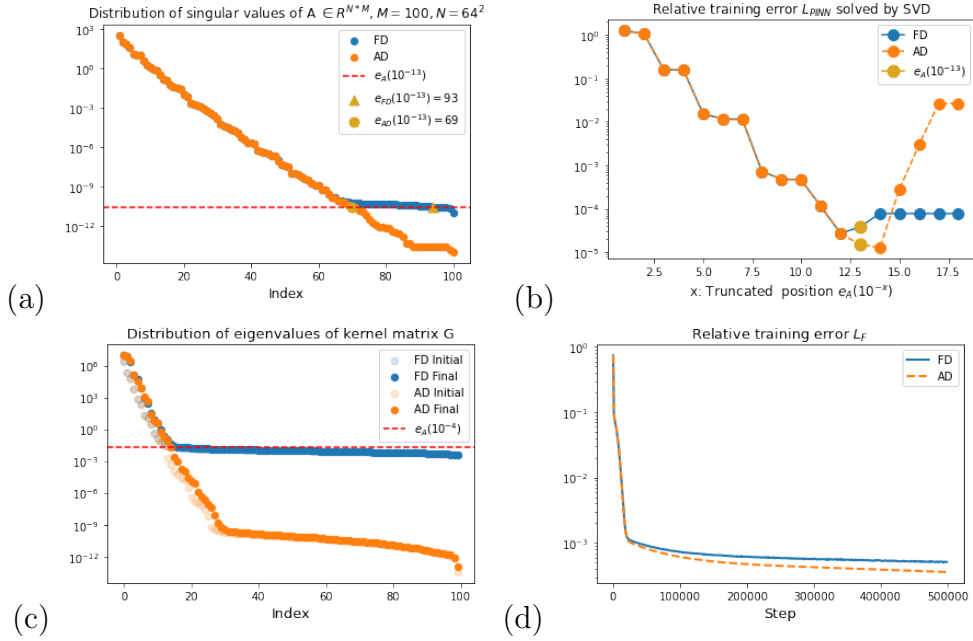


Figure 5: **Poisson Equation in 2D.** (a): Distribution of singular values of the random feature matrix  $\mathbf{A}_k$  with the red dashed line indicating the effective cut-off number is  $e_{G_k}(10^{-13})$ . The *truncated entropy* values are  $H_{\mathbf{A}_{\text{FD}}}(10^{-13}) = 0.3122$  and  $H_{\mathbf{A}_{\text{AD}}}(10^{-13}) = 0.3342$ . (b): Relative training error of  $L_{\text{PINN}}$ , denoted as  $\frac{\|\mathbf{A}_k \mathbf{a} - \mathbf{f}\|}{\|\mathbf{f}\|}$ , obtained using the truncated SVD method. The horizontal axis represents the truncation position determined by the effective cut-off number. (c): Distribution of eigenvalues of kernel matrix  $G$  with the red dashed line indicating the approximate convergence position  $e_{G_k}(10^{-4})$  at the end of training. The *truncated entropy* values are  $H_{G_{\text{FD}}}(10^{-4}) = 0.3336$  and  $H_{G_{\text{AD}}}(10^{-4}) = 0.4460$ . (d): Training curve of relative training error  $\frac{L_F}{\|\mathbf{f}\|}$ .

As shown in Fig. 5 it can be observed that the distribution of singular values of matrix  $\mathbf{A}$  in the RFM and the distribution of eigenvalues of matrix  $\mathbf{G}$  in the NN exhibit the same relationship between the AD and FD methods as described in the previous analysis. By comparing with the 1D scenario, it can be observed that the difference in truncated entropy between AD and FD is not significant, resulting in a similar training error. However, AD still outperforms FD.

**Biharmonic Equation.** We consider the fourth-order two-point boundary value problem

$$\frac{d^4 u(x)}{d^4 x} = \exp(x) \quad (33)$$

with boundary conditions  $u(-1) = u(1) = 0$  and  $u'(-1) = u'(1) = 0$ . The exact solution is  $u(x) = c_0 + c_1 x + c_2 x^2 + c_3 x^3 + \exp(x)$  with  $c_0 = -\frac{5}{12}e^{-1} - \frac{1}{4}e$ ,  $c_1 = \frac{1}{2}e^{-1} - \frac{1}{2}e$ ,  $c_2 = \frac{1}{4}e^{-1} - \frac{1}{4}e$ ,  $c_3 = -\frac{1}{3}e^{-1}$ . In 2D Poisson equation, the loss functions  $L_{\text{PINN}}^{\text{AD}}(\boldsymbol{\theta})$  and  $L_{\text{PINN}}^{\text{FD}}(\boldsymbol{\theta})$  are defined as follow:

$$\begin{aligned} L_{\text{PINN}}^{\text{AD}}(\boldsymbol{\theta}) &:= L_{\text{F}}^{\text{AD}}(\theta) + \lambda L_{\text{B}}(\theta) \\ &= \frac{1}{N} \sum_{i=1}^N |\phi_{xxxx}(x_i; \boldsymbol{\theta}) - f(\mathbf{x})|^2 + \lambda \frac{1}{\hat{N}} \left( \sum_{i=1}^{\hat{N}} |\phi(y_i; \boldsymbol{\theta})|^2 + \sum_{i=1}^{\hat{N}} |\phi_x(y_i; \boldsymbol{\theta})|^2 \right), \end{aligned} \quad (34)$$

$$\begin{aligned} L_{\text{PINN}}^{\text{FD}}(\boldsymbol{\theta}) &:= L_{\text{F}}^{\text{FD}}(\theta) + \lambda L_{\text{B}}(\theta) \\ &= \frac{1}{N} \sum_{i=1}^N \left| \frac{\phi_{i-2} - 4\phi_{i-1} + 6\phi_i - 4\phi_{i+1} + \phi_{i+2}}{h^4} - f(x_i) \right|^2 \\ &\quad + \lambda \frac{1}{\hat{N}} \left( \sum_{i=1}^{\hat{N}} |\phi(y_i; \boldsymbol{\theta})|^2 + \sum_{i=1}^{\hat{N}} |\phi_x(y_i; \boldsymbol{\theta})|^2 \right), \end{aligned} \quad (35)$$

where  $\lambda = 100$  and  $h = \frac{2}{64}$  and  $\phi_i := \phi(x_i; \boldsymbol{\theta})$ .

Due to the high order derivatives, the difference in the singular values distribution of  $\mathbf{A}$  and eigenvalue distribution of  $\mathbf{G}$  between AD and FD becomes more pronounced, as shown in Fig. 6. This leads to a larger difference in truncated entropy and thus AD significantly outperforms FD.

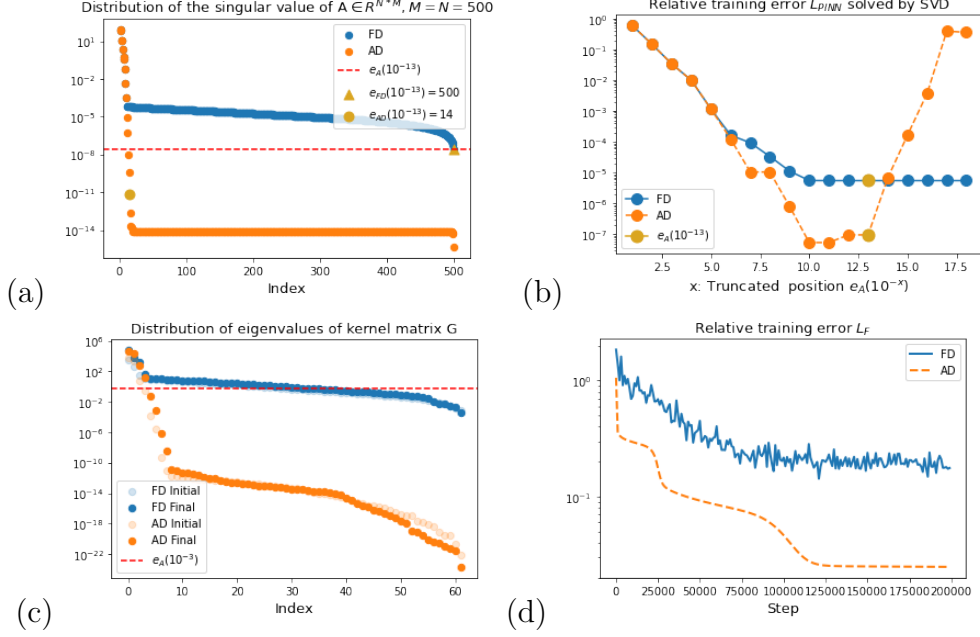


Figure 6: **Bi-harmonic Equation.** (a): Distribution of singular values of the random feature  $A_k$  with the red dashed line indicating the effective cut-off number is  $e_{G_k}(10^{-13})$ . The *truncated entropy* values are  $H_{A_{FD}}(10^{-13}) = 0.1895$  and  $H_{A_{AD}}(10^{-13}) = 0.4460$ . (b): Relative training error of  $L_{PINN}$ , denoted as  $\frac{\|A_k a - f\|}{\|f\|}$ , obtained using the truncated SVD method. The horizontal axis represents the truncation position determined by the effective cut-off number. (c): Distribution of eigenvalues of kernel matrix  $G$  with the red dashed line indicating the approximate convergence position  $e_{G_k}(10^{-2})$  at the end of training. The *truncated entropy* values are  $H_{G_{FD}}(10^{-2}) = 0.5058$  and  $H_{G_{AD}}(10^{-2}) = 0.6720$ . (d): Training curve of relative training error  $\frac{L_F}{\|f\|}$ .

## 5. Conclusions and Discussions

In this paper, we study the performance of AD and FD methods in training neural network structures to solve PDEs, including random feature models and two-layer neural networks. Our paper is the first to compare AD and FD from a training perspective theoretically and numerically. Our analysis of eigenvalues shows that the small eigenvalues of AD are smaller than those of FD methods, leading to superior performance in both SVD for random

feature models and gradient descent for neural networks. To describe the influence of eigenvalues on training error, we introduce the concepts of *Effective cut-off number* and *Truncated entropy*, observing that larger *Truncated entropy* corresponds to smaller training error. Based on our findings, under the same settings, the truncated entropy of AD is larger than that of FD, predicting that AD outperforms FD methods in the training process. This analysis can extend to general neural network training scenarios, with *Truncated entropy* as an indicator of loss convergence speed.

Our analysis is based on PINNs with random feature networks and two-layer neural networks. We chose these models as a starting point for our investigation due to their simplicity and ease of analysis. The same analytical techniques and phenomena can be extended to deeper neural network structures, such as Random neural networks and deeper fully connected neural networks. We provide an example in the appendix. Exploring the properties of solving PDEs using different neural network architectures such as Convolutional Neural Networks (CNN) and Transformers can be considered as future work. In neural network methods for solving PDEs, the error can be divided into three components: approximation error, generalization error, and training error. Our paper focuses on the training error introduced by differential methods, distinct from approximation and generalization errors. The relative error against a ground truth solution decreases as the training error decreases. (Checked in the appendix.) This provides insights into how to train the loss function when derivative information is included effectively. Based on our findings, incorporating preconditioners into optimization algorithms could accelerate the convergence of training errors. Further research can be done to investigate the most suitable preconditioners for different PDE types and neural network architectures.

## Acknowledgements

Y.Y. and W.H. was supported by National Institute of General Medical Sciences through grant 1R35GM146894. The work of Y.X. was supported by the Project of Hetao Shenzhen-HKUST Innovation Cooperation Zone HZQB-KCZYB-2020083.

## Declaration of generative AI and AI-assisted technologies in the writing process

During the preparation of this work the author(s) used ChatGPT in order to improve language and readability. After using this tool/service, the author(s) reviewed and edited the content as needed and take(s) full responsibility for the content of the publication.

## References

- [1] M. Raissi, P. Perdikaris, G. Karniadakis, Physics-informed neural networks: A deep learning framework for solving forward and inverse problems involving nonlinear partial differential equations, *Journal of Computational Physics* 378 (2019) 686–707.
- [2] B. Yu, et al., The deep ritz method: a deep learning-based numerical algorithm for solving variational problems, *Communications in Mathematics and Statistics* 6 (1) (2018) 1–12.
- [3] J. Han, A. Jentzen, W. E, Solving high-dimensional partial differential equations using deep learning, *Proceedings of the National Academy of Sciences* 115 (34) (2018) 8505–8510.
- [4] J. Siegel, Q. Hong, X. Jin, W. Hao, J. Xu, Greedy training algorithms for neural networks and applications to pdes, *Journal of Computational Physics* 484 (2023) 112084.
- [5] Q. Hong, J. Siegel, J. Xu, A priori analysis of stable neural network solutions to numerical pdes, *arXiv preprint arXiv:2104.02903* (2021).
- [6] S. Cao, Choose a transformer: Fourier or galerkin, *Advances in neural information processing systems* 34 (2021) 24924–24940.
- [7] J. Chen, X. Chi, Z. Yang, et al., Bridging traditional and machine learning-based algorithms for solving pdes: the random feature method, *J Mach Learn* 1 (2022) 268–98.
- [8] Y. Lan, Z. Li, J. Sun, Y. Xiang, Dosnet as a non-black-box pde solver: When deep learning meets operator splitting, *Journal of Computational Physics* 491 (2023) 112343. doi:<https://doi.org/10.1016/j.jcp.2023.112343>.

URL <https://www.sciencedirect.com/science/article/pii/S0021999123004382>

- [9] D. R., S. Mishra, Error analysis for physics-informed neural networks (pinns) approximating kolmogorov pdes, *Advances in Computational Mathematics* 48 (6) (2022) 79.
- [10] Y. Yang, J. He, Deeper or wider: A perspective from optimal generalization error with sobolev loss, *International Conference on Machine Learning* (2024).
- [11] J. Lu, Z. Shen, H. Yang, S. Zhang, Deep network approximation for smooth functions, *SIAM Journal on Mathematical Analysis* 53 (5) (2021) 5465–5506.
- [12] A. Baydin, B. Pearlmutter, A. Radul, J. Siskind, Automatic differentiation in machine learning: a survey, *Journal of machine learning research* 18 (153) (2018) 1–43.
- [13] P.-H. Chiu, J. C. Wong, C. Ooi, M. H. Dao, Y.-S. Ong, Canpinn: A fast physics-informed neural network based on coupled-automatic-numerical differentiation method, *Computer Methods in Applied Mechanics and Engineering* 395 (2022) 114909. doi:<https://doi.org/10.1016/j.cma.2022.114909>.  
URL <https://www.sciencedirect.com/science/article/pii/S0045782522001906>
- [14] C. Grossmann, *Numerical treatment of partial differential equations*, Springer, 2007.
- [15] R. G. Patel, I. Manickam, N. A. Trask, M. A. Wood, M. Lee, I. Tomas, E. C. Cyr, Thermodynamically consistent physics-informed neural networks for hyperbolic systems, *Journal of Computational Physics* 449 (2022) 110754. doi:<https://doi.org/10.1016/j.jcp.2021.110754>.  
URL <https://www.sciencedirect.com/science/article/pii/S0021999121006495>
- [16] K. L. Lim, R. Dutta, M. Rotaru, Physics informed neural network using finite difference method, in: *2022 IEEE International Conference on Systems, Man, and Cybernetics (SMC)*, IEEE, 2022, pp. 1828–1833.

- [17] T. Praditia, M. Karlbauer, S. Otte, S. Oladyshkin, M. V. Butz, W. Nowak, Finite volume neural network: Modeling subsurface contaminant transport, arXiv preprint arXiv:2104.06010 (2021).
- [18] N. Wandel, M. Weinmann, R. Klein, Learning incompressible fluid dynamics from scratch—towards fast, differentiable fluid models that generalize, arXiv preprint arXiv:2006.08762 (2020).
- [19] N. Wandel, M. Weinmann, R. Klein, Teaching the incompressible navier–stokes equations to fast neural surrogate models in three dimensions, *Physics of Fluids* 33 (4) (2021).
- [20] H. Gao, L. Sun, J.-X. Wang, Phygeonet: Physics-informed geometry-adaptive convolutional neural networks for solving parameterized steady-state pdes on irregular domain, *Journal of Computational Physics* 428 (2021) 110079.
- [21] P.-H. Chiu, J. C. Wong, C. Ooi, M. H. Dao, Y.-S. Ong, Can-pinn: A fast physics-informed neural network based on coupled-automatic–numerical differentiation method, *Computer Methods in Applied Mechanics and Engineering* 395 (2022) 114909.
- [22] O. Roy, M. Vetterli, The effective rank: A measure of effective dimensionality, in: 2007 15th European signal processing conference, IEEE, 2007, pp. 606–610.
- [23] D. Frenkel, B. Smit, *Understanding molecular simulation: from algorithms to applications*, Elsevier, 2023.
- [24] A. Barron, Universal approximation bounds for superpositions of a sigmoidal function, *IEEE Transactions on Information theory* 39 (3) (1993) 930–945.
- [25] H. Mhaskar, Neural networks for optimal approximation of smooth and analytic functions, *Neural computation* 8 (1) (1996) 164–177.
- [26] J. Lu, Y. Lu, M. Wang, A priori generalization analysis of the Deep Ritz method for solving high dimensional elliptic partial differential equations, in: *Conference on Learning Theory*, PMLR, 2021, pp. 3196–3241.



- [27] Y. Yang, H. Yang, Y. Xiang, Nearly optimal vc-dimension and pseudo-dimension bounds for deep neural network derivatives, *Advances in Neural Information Processing Systems* 36 (2024).
- [28] A. Rahimi, B. Recht, Uniform approximation of functions with random bases, in: *2008 46th annual allerton conference on communication, control, and computing*, IEEE, 2008, pp. 555–561.
- [29] A. Rahimi, B. Recht, Weighted sums of random kitchen sinks: Replacing minimization with randomization in learning, *Advances in neural information processing systems* 21 (2008).
- [30] K. W. Morton, D. F. Mayers, *Numerical solution of partial differential equations: an introduction*, Cambridge university press, 2005.
- [31] S. Ruder, An overview of gradient descent optimization algorithms, *arXiv preprint arXiv:1609.04747* (2016).
- [32] M. Zinkevich, M. Weimer, L. Li, A. Smola, Parallelized stochastic gradient descent, *Advances in neural information processing systems* 23 (2010).
- [33] D. Kingma, J. Ba, Adam: A method for stochastic optimization, *arXiv preprint arXiv:1412.6980* (2014).
- [34] W. Hao, Q. Hong, X. Jin, Y. Wang, Gauss newton method for solving variational problems of pdes with neural network discretizations, *arXiv preprint arXiv:2306.08727* (2023).
- [35] H. He, Z. Tang, S. Zhao, Y. Saad, Y. Xi, nltgcr: A class of nonlinear acceleration procedures based on conjugate residuals, *SIAM Journal on Matrix Analysis and Applications* 45 (1) (2024) 712–743.
- [36] Y. Yang, Q. Chen, W. Hao, Homotopy relaxation training algorithms for infinite-width two-layer relu neural networks, *arXiv preprint arXiv:2309.15244* (2023).

## Appendix

### Appendix A. Experimental Details

In this section, we include more details about the experiments shown in the main text. We describe the experimental details based on different equations.

#### Appendix A.1. Training setting

In the case of the random feature model, the system precision is set to double, while for the neural network model, the system precision is set to float. We train neural networks using the SGD optimizer with full batch training. We perform a learning rate sweep ranging from 1e-3 to 1e-4. All random feature models are structured as 2-layer fully connected NN, a  $\sin(x)$  activation function, and with  $\mathbf{w}_j \sim \mathbb{U}([-1, 1]^d)$  and  $b_j \sim \mathbb{U}([-1, 1])$ . All neural networks are 2-layer fully connected NN, a  $\sin(x)$  activation function, and uniformly sample collocation points  $x$  on the domain. All experiments are run on a single NVIDIA 3070Ti GPU.

#### Appendix A.2. Poisson Equation in 1D

**Equation.**

$$\begin{cases} u_{xx}(x) = f(x), & x \in [-1, 1], \\ u(-1) = u(1) = 0. \end{cases} \quad (\text{A.2.1})$$

By choosing  $f(x) = -\pi^2 \sin(\pi x)$ , we have the exact solution is  $u(x) = \sin(\pi x)$ .

**Random feature models.** We include extra distribution of singular values of  $A_{\text{AD}}$  and  $A_{\text{FD}}$  for different  $M = N$  as shown in Fig. 1 in the main context. The activation function is  $\sin(x)$ .

**Neural Network.** As shown in Fig. 4 in the main context. Here, we use 2-layer fully connected NN with 100 neurons per layer, a  $\sin(x)$  activation function, and uniformly 100 sample collocation points. The loss function for AD and FD are defined as followed:

$$L_{\text{PINN}}^{\text{AD}}(\boldsymbol{\theta}) := L_{\text{F}}^{\text{AD}}(\boldsymbol{\theta}) + \lambda L_{\text{B}}(\boldsymbol{\theta}) = \frac{1}{N} \sum_{i=1}^N |\Delta \phi(\mathbf{x}_i; \boldsymbol{\theta}) - f(\mathbf{x})|^2 + \lambda \frac{1}{\hat{N}} \sum_{i=1}^{\hat{N}} |\phi(\mathbf{y}_i; \boldsymbol{\theta})|^2, \quad (\text{A.2.2})$$

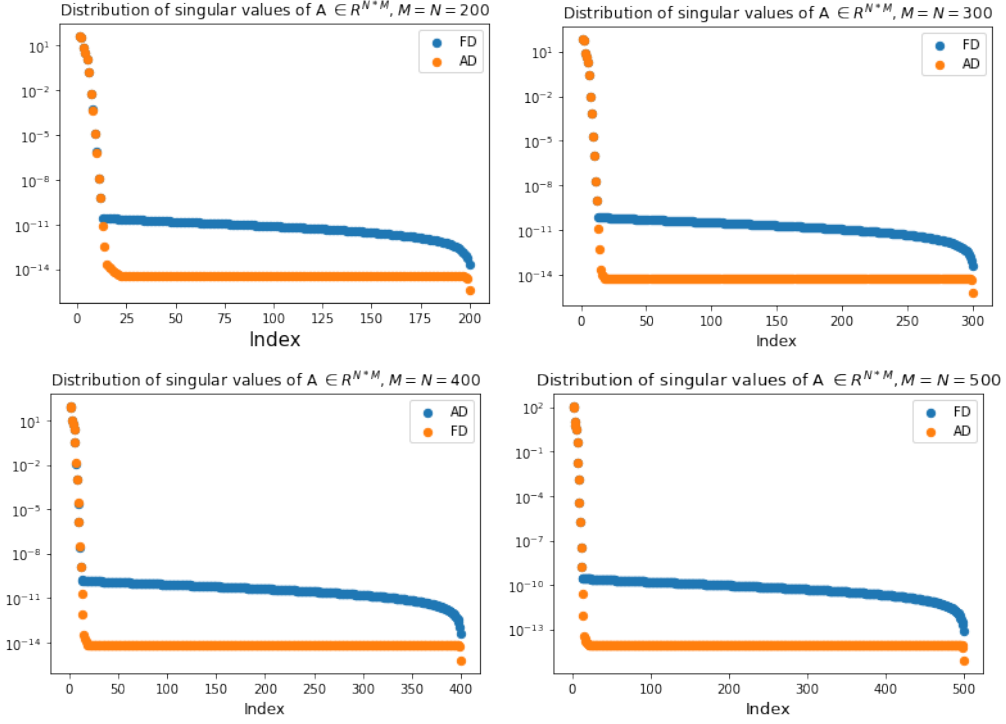


Figure A.2.1: Distribution of singular values of  $\mathbf{A}_{\text{AD}}$  and  $\mathbf{A}_{\text{FD}}$  for different settings of  $M = N$ .

$$\begin{aligned}
 L_{\text{PINN}}^{\text{FD}}(\boldsymbol{\theta}) &:= L_{\text{F}}^{\text{FD}}(\boldsymbol{\theta}) + \lambda L_{\text{B}}(\boldsymbol{\theta}) \\
 &= \frac{1}{N} \sum_{i=1}^N \left| \frac{\phi(x_{i-1}; \boldsymbol{\theta}) + \phi(x_{i+1}; \boldsymbol{\theta}) - 2\phi(x_i; \boldsymbol{\theta})}{h^2} - f(x_i) \right|^2 + \lambda \frac{1}{\hat{N}} \sum_{i=1}^{\hat{N}} |\phi(\mathbf{y}_i; \boldsymbol{\theta})|^2,
 \end{aligned}
 \tag{A.2.3}$$

where  $\lambda = 1$  and  $h = \frac{2}{100}$ .

### Appendix A.3. Poisson Equation in 2D.

**Equation.**

$$\begin{cases} \Delta u(x, y) = f(x, y), & (x, y) \in \Omega, \\ u(x, y) = 0, & (x, y) \in \partial\Omega. \end{cases}
 \tag{A.3.1}$$

By choosing  $f(x) = -\pi^2 \sin(\pi x) \sin(\pi y)$ , we have the exact solution is  $u(x, y) = \sin(\pi x) \sin(\pi y) \in [0, 1] \times [0, 1]$ .

**Random Feature Models.** In this case the  $M = 100, N = 64 \times 64$   
 $\mathbf{A}_{\text{FD}} = \mathbf{C} \cdot \mathbf{A}_0$ .

$$\mathbf{C} = \frac{1}{h^2} \begin{bmatrix} D & -I & 0 & 0 & 0 & \cdots & 0 \\ -I & D & -I & 0 & 0 & \cdots & 0 \\ 0 & -I & D & -I & 0 & \cdots & 0 \\ \vdots & \ddots & \ddots & \ddots & \ddots & \ddots & \vdots \\ 0 & \cdots & 0 & -I & D & -I & 0 \\ 0 & \cdots & \cdots & 0 & -I & D & -I \\ 0 & \cdots & \cdots & \cdots & 0 & -I & D \end{bmatrix}$$

$I$  is the  $64 \times 64$  identity matrix, and  $D$ , also  $64 \times 64$ , is given by:

$$D = \begin{bmatrix} 4 & -1 & 0 & 0 & 0 & \cdots & 0 \\ -1 & 4 & -1 & 0 & 0 & \cdots & 0 \\ 0 & -1 & 4 & -1 & 0 & \cdots & 0 \\ \vdots & \ddots & \ddots & \ddots & \ddots & \ddots & \vdots \\ 0 & \cdots & 0 & -1 & 4 & -1 & 0 \\ 0 & \cdots & \cdots & 0 & -1 & 4 & -1 \\ 0 & \cdots & \cdots & \cdots & 0 & -1 & 4 \end{bmatrix}.$$

**Neural Network.** As shown in Fig. 5 in the main context. Here, we use 2-layer fully connected NN with 100 neurons per layer, a  $\sin(x)$  activation function, and uniformly  $N = 64 \times 64$  sample collocation points. The loss function for AD and FD are defined as followed:

$$L_{\text{PINN}}^{\text{AD}}(\boldsymbol{\theta}) := L_{\text{F}}^{\text{AD}}(\boldsymbol{\theta}) + \lambda L_{\text{B}}(\boldsymbol{\theta}) = \frac{1}{N} \sum_{i=1}^N |\Delta \phi_{xx}(x_i; \boldsymbol{\theta}) - f(\mathbf{x})|^2 + \lambda \frac{1}{\hat{N}} \sum_{i=1}^{\hat{N}} |\phi(\mathbf{y}_i; \boldsymbol{\theta})|^2, \quad (\text{A.3.2})$$

$$\begin{aligned} L_{\text{PINN}}^{\text{FD}}(\boldsymbol{\theta}) &:= L_{\text{F}}^{\text{FD}}(\boldsymbol{\theta}) + \lambda L_{\text{B}}(\boldsymbol{\theta}) \\ &= \frac{1}{N} \sum_{i=1}^N \left| \frac{\phi_{i+1,j} + \phi_{i-1,j} + \phi_{i,j-1} + \phi_{i,j+1} - e\phi_{i,j}}{h^2} - f(x_i) \right|^2 + \lambda \frac{1}{\hat{N}} \sum_{i=1}^{\hat{N}} |\phi(\mathbf{y}_i; \boldsymbol{\theta})|^2, \end{aligned} \quad (\text{A.3.3})$$

where  $\lambda = 1$  and  $h = \frac{1}{64}$  and  $\phi_{i,j} := \phi((x_i, y_j); \boldsymbol{\theta})$ .

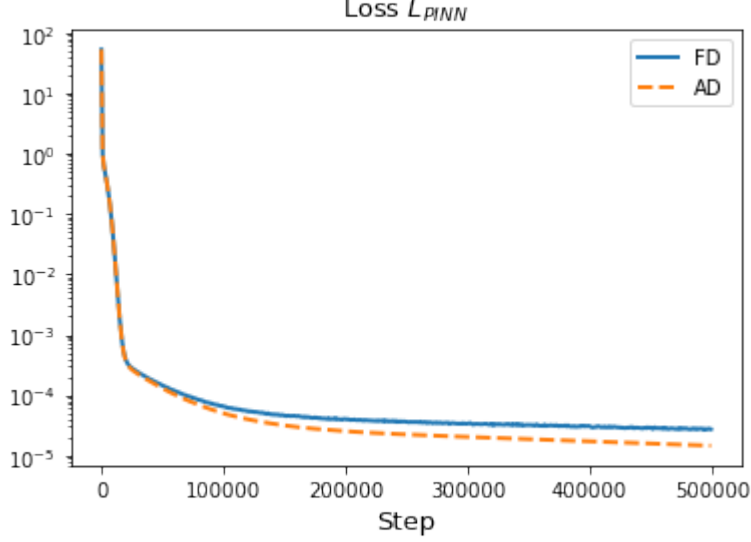


Figure A.3.1: Training curve of the loss function  $L_{\text{PINN}}$ .

#### Appendix A.4. Biharmonic Equation.

##### Equation

$$\frac{d^4 u(x)}{d^4 x} = \exp(x), \quad (\text{A.4.1})$$

with boundary conditions  $u(-1) = u(1) = 0$  and  $u'(-1) = u'(1) = 0$ . The exact solution is  $u(x) = c_0 + c_1 x + c_2 x^2 + c_3 x^3 + \exp(x)$  with  $c_1 = -\frac{5}{12}e^{-1} - \frac{1}{4}e$ ,  $c_2 = \frac{1}{2}e^{-1} - \frac{1}{2}e$ ,  $c_3 = \frac{1}{4}e^{-1} - \frac{1}{4}e$ ,  $c_0 = -\frac{1}{3}e^{-1}$ .

**Random feature models.** In this case the  $M = N = 500$   $\mathbf{A}_{\text{FD}} = \mathbf{C} \cdot \mathbf{A}_0$

$$C = \frac{1}{h^4} \begin{bmatrix} -4 & 6 & -4 & 0 & 0 & \cdots & 0 \\ 1 & -4 & 6 & -4 & 1 & \cdots & 0 \\ 0 & 1 & -4 & 6 & -4 & \cdots & 0 \\ \vdots & \ddots & \ddots & \ddots & \ddots & \ddots & \vdots \\ 0 & \cdots & 4 & -6 & 4 & 1 & 0 \\ 0 & \cdots & \cdots & 4 & -6 & 4 & 1 \\ 0 & \cdots & \cdots & \cdots & 4 & -6 & 4 \end{bmatrix}$$

**Neural Network.** As shown in Fig. 5 in the main context. Here, we use 2-layer fully connected NN with 100 neurons per layer, a  $\sin(x)$  activation

function, and uniformly  $N = 64 \times 64$  sample collocation points. The loss function for AD and FD are defined as followed:

$$\begin{aligned}
L_{\text{PINN}}^{\text{AD}}(\boldsymbol{\theta}) &:= L_{\text{F}}^{\text{AD}}(\theta) + \lambda L_{\text{B}}(\theta) \\
&= \frac{1}{N} \sum_{i=1}^N |\phi_{xxx}(x_i; \boldsymbol{\theta}) - f(\mathbf{x})|^2 + \lambda \frac{1}{\hat{N}} \left( \sum_{i=1}^{\hat{N}} |\phi(y_i; \boldsymbol{\theta})|^2 + \sum_{i=1}^{\hat{N}} |\phi_x(y_i; \boldsymbol{\theta})|^2 \right),
\end{aligned} \tag{A.4.2}$$

$$\begin{aligned}
L_{\text{PINN}}^{\text{FD}}(\boldsymbol{\theta}) &:= L_{\text{F}}^{\text{FD}}(\theta) + \lambda L_{\text{B}}(\theta) \\
&= \frac{1}{N} \sum_{i=1}^N \left| \frac{\phi_{i-2} - 4\phi_{i-1} + 6\phi_i - 4\phi_{i+1} + \phi_{i+2}}{h^4} - f(x_i) \right|^2 \\
&\quad + \lambda \frac{1}{\hat{N}} \left( \sum_{i=1}^{\hat{N}} |\phi(y_i; \boldsymbol{\theta})|^2 + \sum_{i=1}^{\hat{N}} |\phi_x(y_i; \boldsymbol{\theta})|^2 \right)
\end{aligned} \tag{A.4.3}$$

where  $\lambda = 100$  and  $h = \frac{1}{64}$  and  $\phi_i := \phi(x_i; \boldsymbol{\theta})$ .

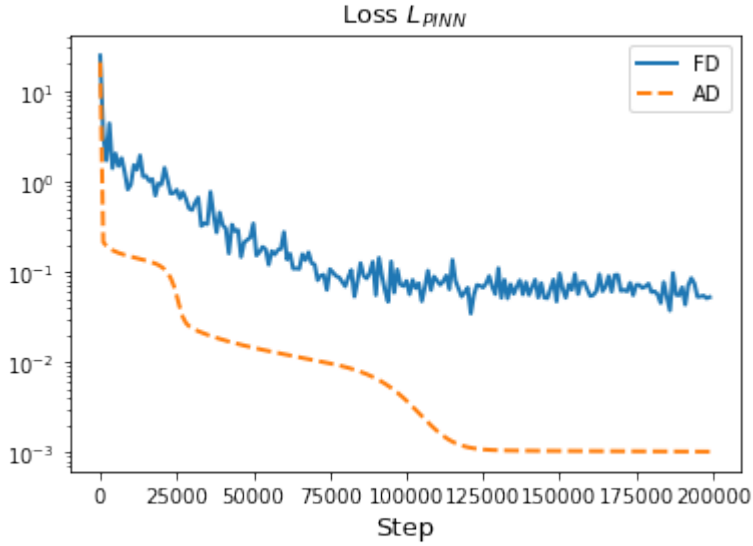


Figure A.4.1: Training curve of the loss function  $L_{\text{PINN}}$ .

## Appendix B. Additional Experiments.

In this section, we present additional experimental results showcasing the outcomes in the case of the 1D Poisson Equation. For different grid sizes  $h$ , the results include the loss curve, the corresponding Relative L2 error curve, and the case of a deeper neural network.

### Appendix B.1. Different Grid Size $h$ .

As shown in Figure B.1, we extend the analysis of eigenvalue distribution for the 1D Poisson equation with  $M = N$  under the Random Feature Model. Results corresponding to **Proposition 1 and 2** in Section 3.1 are applicable across various scenarios.

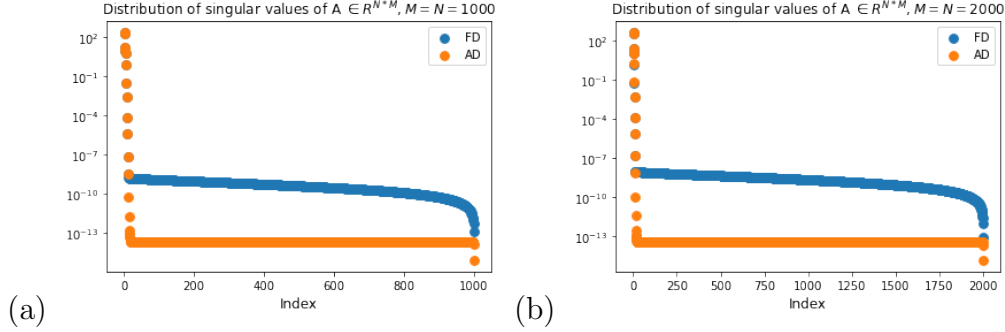


Figure B.1: Distribution of singular values for  $A_{FD}$  and  $A_{AD}$  for solving 1D Poisson equation using Random Feature Method with activation function  $\sigma(x) = \sin(x)$  with vary Number of Sample Points  $N$  and Number of Neurons  $M$ . **(a)**:  $M = N = 1000$ . **(b)**:  $M = N = 2000$ .

### Appendix B.2. Loss Curve and Relative L2 Error

Figure B.2 presents the convergence behavior of the loss curve and the corresponding relative L2 error for the 1D Poisson equation with  $M = N$ . It shows that AD consistently achieves lower training errors and relative errors compared to FD, demonstrating its superior performance in this setting.

### Appendix B.3. Deep neural network.

We conduct experiments on the deep neural network (DNN) case with the structure  $[1, 50, 50, 50, 1]$ , using the activation function  $\tanh(x)$ .

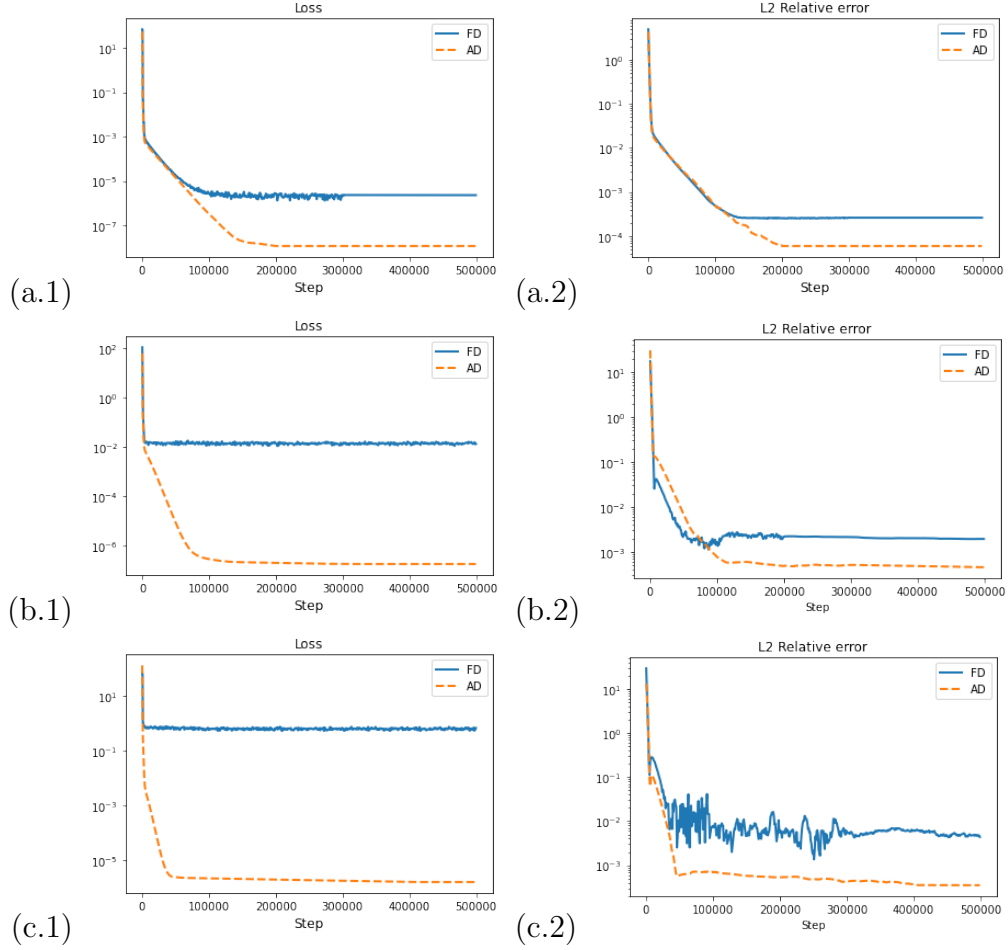


Figure B.2: Training curve of training error  $L$  and its corresponding relative  $L_2$  error.

**Random Neural Network.** Here we chose  $N = 500$ . The results is shown in Figure B.3.1.

**Deep neural network.** Here, we selected  $N = 100$  with the Adam optimization method using full batch training. The results is shown in Figure B.3.2.



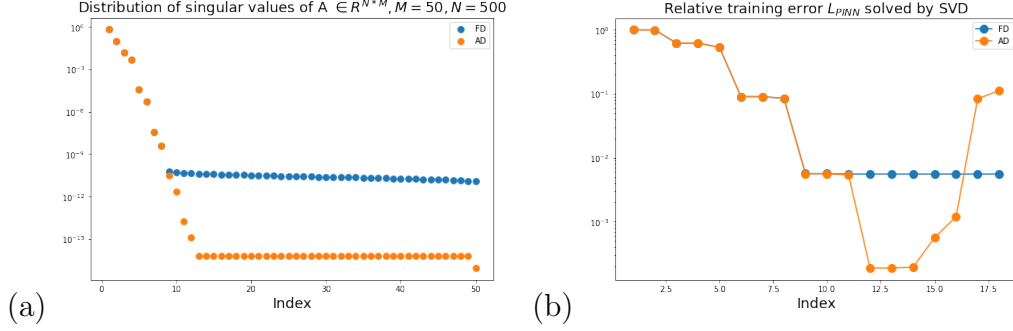


Figure B.3.1: **Random neural network.** (a): Distribution of singular values of the random feature  $\mathbf{A}_k$  with the red dashed line indicating the effective cut-off number is  $e_{G_k}(10^{-13})$ . The *truncated entropy* values are  $H_{\mathbf{A}_{FD}}(10^{-13}) = 0.1098$  and  $H_{\mathbf{A}_{AD}}(10^{-13}) = 0.2197$ . (b): Relative training error of  $L_{PINN}$ , denoted as  $\frac{\|\mathbf{A}_k \mathbf{a} - \mathbf{f}\|}{\|\mathbf{f}\|}$ , obtained using the truncated SVD method. The horizontal axis represents the truncation position determined by the effective cut-off number.

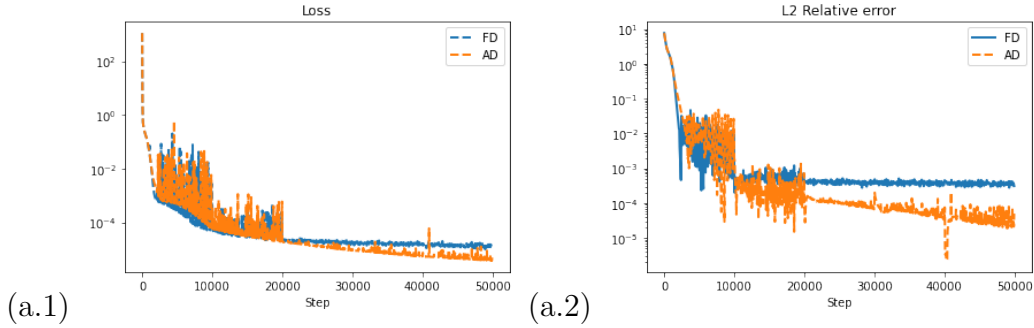


Figure B.3.2: Training curve of training error  $L$  and its corresponding relative  $L_2$  error.